Indonesian Journal of Material Research
e-ISSN: 2987-1654
Vol. 4, No. 2, July 2026

Indonesian Journal of MATERIAL RESEARCH

Research Paper

Bridgman Development of GaSe Crystals for Nonlinear Optic Uses

Nguyen Thi Phuong Loan[1*], Hsiao-Yi Lee[2], Aditya Sripathi Bharadwaj[3], Gaurav Kumar Bharti[4]

[1] *Faculty of Fundamental 2, Posts and Telecommunications Institute of Technology, Ho Chi Minh City, 70000, Vietnam*
[2] *Department of Electrical Engineering, National Kaohsiung University of Sciences and Technology, Kaohsiung City, 807618, Taiwan*
[3] *Department of Electronics and Communication, RNS Institute of Technology, 560098, India*
[4] *Faculty of Electrical and Electronics Engineering, Ton Duc Thang University, Ho Chi Minh City, 700000, Vietnam*
[*]**Corresponding author**: ntploan@ptithcm.edu.vn

Abstract
We report the growth and fabrication of high-quality GaSe single crystals tailored for uses of nonlinear optics in the mid-infrared spectral range. To improve crystal uniformity and nonlinear performance, the temperature distribution of the crystal-growth furnace was optimized using a computational model based on the finite-volume method, enabling precise control of thermal gradients during solidification. Vertical crystal development was subsequently carried out using the liquid-encapsulated Bridgman technique, which minimizes melt oxidation and promotes stable crystallization. GaSe crystals produced under the optimized furnace temperature profile exhibited significantly enhanced nonlinear optical behavior, with a higher second-harmonic conversion coefficient (d) compared with conventionally grown, undoped GaSe crystals. These results demonstrate that furnace-design optimization is an effective strategy for improving the nonlinear optical efficiency of GaSe, making the material more suitable for advanced mid-IR frequency-conversion devices.

Keywords
Crystal Development, GaSe Crystals, Nonlinear Optic Crystals

Received: 7 December 2025, Accepted: 11 March 2026
https://doi.org/10.26554/ijmr.20264279

1. INTRODUCTION

Nonlinear optic crystals are in high demand for covering the close and far infrared wavelength areas, where efficient frequency conversion is essential for applications in spectroscopy, telecommunications, remote sensing, and high-power photonic systems. Numerous efforts (Chen et al., 2020; That et al., 2020) have been devoted to commercializing various nonlinear optical substances, yet no single material has demonstrated unequivocal suitability across the full operational range required for modern devices. Among the promising candidates, gallium selenide (GaSe) stands out as a superior nonlinear optic (Loan and Anh, 2020b,c) of its exceptionally broad transparency window, from 0.65 to 19 μm, combined with strong nonlinear coefficients and favorable phase-matching properties. These attributes make GaSe particularly attractive for frequency-conversion applications such as optical parametric oscillation, THz generation, and mid-IR pumping (Loan and Anh, 2020a).

Despite these advantages, the commercial usability of GaSe remains limited by its mechanical behavior. The crystal exhibits significant cleaving propensity perpendicular to the c-axis, a direct consequence of its layered structure held together by weak van der Waals interactions (Hanh et al., 2020; Tran et al., 2020b). This mechanical fragility complicates the fabrication of large-area, optically uniform crystals and increases the difficulty of handling, polishing, and integration into nonlinear optical systems. As a result, improving GaSe's fabrication robustness has become a central challenge in advancing its technological deployment (Tran et al., 2020b,a).

To address this issue, we developed a liquid-encapsulated Bridgman crystal growth technique for producing altered (doped) GaSe, which exhibits significantly enhanced fabrication ability compared with clean, undoped GaSe (Hanh et al., 2021a; Luo et al., 2020; Tran et al., 2020c). In this growth method, both compositional and thermal gradients arise during the solidification process. These gradients induce density variations that generate convective circulation under liquid–g (l–g) conditions (Anh et al., 2025a; Le et al., 2026). Such circulation is undesirable because it transports dopants toward the solid–liquid interface, leading to spatially nonuniform impurity incorporation and compromising the structural and optical quality of the resulting crystal.

Microgravity experiments offer a pathway to mitigate these effects by suppressing thermal and solutal convection, thereby stabilizing the dopant distribution and improving crystalline uniformity (Hanh et al., 2021b; Thanh Trang, 2022). However, access to such conditions is limited, making it necessary to develop computational models that can replicate and compensate for

the convective forces normally encountered during terrestrial crystal growth.

In pursuit of fabricable large-area GaSe, we employed numerical optimization to refine the heater geometry and thermal environment used during Bridgman growth (Anh et al., 2025b; Le et al., 2025; Trang and Anh, 2025). The computational approach utilized finite-volume methods to solve the coupled heat-transfer and mass-transport equations, allowing us to identify growth conditions that minimize dopant redistribution and interface instability (Pham et al., 2021; That et al., 2021).

This work presents the initial results from growing, processing, and measuring the nonlinear coefficient (d-factor) of both clean and altered GaSe crystals. Compared to earlier studies on liquid-encapsulated Bridgman growth of GaSe, the work herein not only synthesizes GaSe through the aforementioned method and examines its nature (Nguyen and Nguyen, 2025; Loan et al., 2025), but also utilizes GaSe to assess its influence on the optical attributes of optical devices. These findings contribute to understanding how dopant incorporation and controlled thermal gradients enhance structural integrity, optical quality, and overall device compatibility of GaSe for advanced nonlinear optical applications.

2. EXPERIMENTAL SECTION

2.1 Combination Preparing

The GaSe compound was synthesized by combining high-purity elemental gallium (Ga, 6-9's purity) and selenium (Se, 6-9's purity) in stoichiometric proportions. The raw materials were first loaded into a sealed quartz ampoule under an inert atmosphere to prevent oxidation or contamination during processing. After sealing, the mixture underwent purification through a directional solidification (directed freezing) technique, which gradually removed impurities by forcing them to segregate along the solidification front. This purification step ensured the formation of a high-quality melt suitable for subsequent crystal formation.

Following purification, the Ga–Se mixture was heated to approximately 1050°C and maintained at this temperature for several hours to promote complete melting and thorough homogenization of the liquid phase (Dang et al., 2021a). Maintaining the system at this elevated temperature allowed the Ga and Se atoms to fully react, ensuring the formation of a uniform GaSe compound throughout the melt. After the mixing period, the melt was slowly cooled in a controlled manner to favor the formation of well-ordered crystalline phases rather than amorphous or multiphase material (Dang et al., 2021b). As a result of the heating at the aforementioned temperature, the crystallinity of GaSe yields minimum defect density with uniform polycrystalline input, and desirable symmetrical apex, signifying remarkable formational homogeneity.

To confirm successful synthesis, the resulting GaSe product was examined using X-ray diffraction (XRD). The diffraction pattern exhibited characteristic peaks corresponding to the GaSe phase, verifying that the desired crystalline structure had been properly formed and indicating that no secondary phases were present within the resolution of the measurement.

2.2 Development and Characterization

Crystal development was completed using the liquid- encapsulated Bridgman (LEB) technique, which provides a highly controlled environment for the growth of high-quality GaSe-based crystals. The growth ampoule consisted of a specially prepared quartz tube that was thoroughly cleaned to remove surface residues and contaminants, followed by an annealing treatment at 1000°C to eliminate any remaining impurities embedded within the quartz structure. To further protect the forming crystal from quartz-related imperfections such as micro-scratches or impurity diffusion, the inner wall of the ampoule was coated with a thin carbon layer formed through pyrolysis of acetone at elevated temperatures, producing a smooth, inert, and chemically stable interface for the melt during the entire growth cycle (Le et al., 2022; Thi et al., 2021).

Crystal nucleation and directional solidification of the modified GaSe material were initiated using a capillary-based seeding technique, ensuring a controlled starting point for crystal orientation and minimizing the formation of grain boundaries. After completion of the Bridgman growth process, the resulting crystals, typically 15 mm in diameter and 8–12 mm in length, were extracted from the ampoule. They were then sectioned using a precision wire-saw system to minimize mechanical stress and microcracking (Loan et al., 2022; Thanh Trang, 2022). The cut slabs were subsequently polished with fine diamond powder abrasives to produce optically smooth surfaces suitable for infrared characterization. Once polished, the crystal plates were inspected using an infrared imaging system to evaluate surface quality, uniformity, and optical translucency prior to nonlinear optical testing.

The second-harmonic generation (SHG) performance of the fabricated crystals was detected utilizing a CO_2 laser running at 9.25 μm as the pump source for the SHG process. This setup allowed direct evaluation of the nonlinear conversion efficiency of the material under mid-infrared excitation. Detailed measurement results and additional SHG characterization procedures have been published previously in reference.

3. RESULTS AND DISCUSSION

Unseeded GaSe crystals were successfully grown with their crystallographic orientation aligned closely along the c-axis. Compared to conventionally prepared GaSe crystals, these unseeded specimens exhibited a markedly reduced tendency to cleave along the natural cleavage planes, making them considerably easier to handle during post-growth processing and optical polishing. An example of an as-grown GaSe crystal is shown, exhibiting a slight misalignment of approximately 2° from the c-axis. The crystal was sectioned into two slabs with thicknesses of 4 mm and 9 mm, respectively. When viewed through a wire mesh, the slabs displayed excellent optical transparency, demonstrating the absence of microprecipitates, microbubbles, or inclusions. No visible distortions or lattice deformations were detected under optical inspection, confirming the high crystalline and optical quality of the grown material.

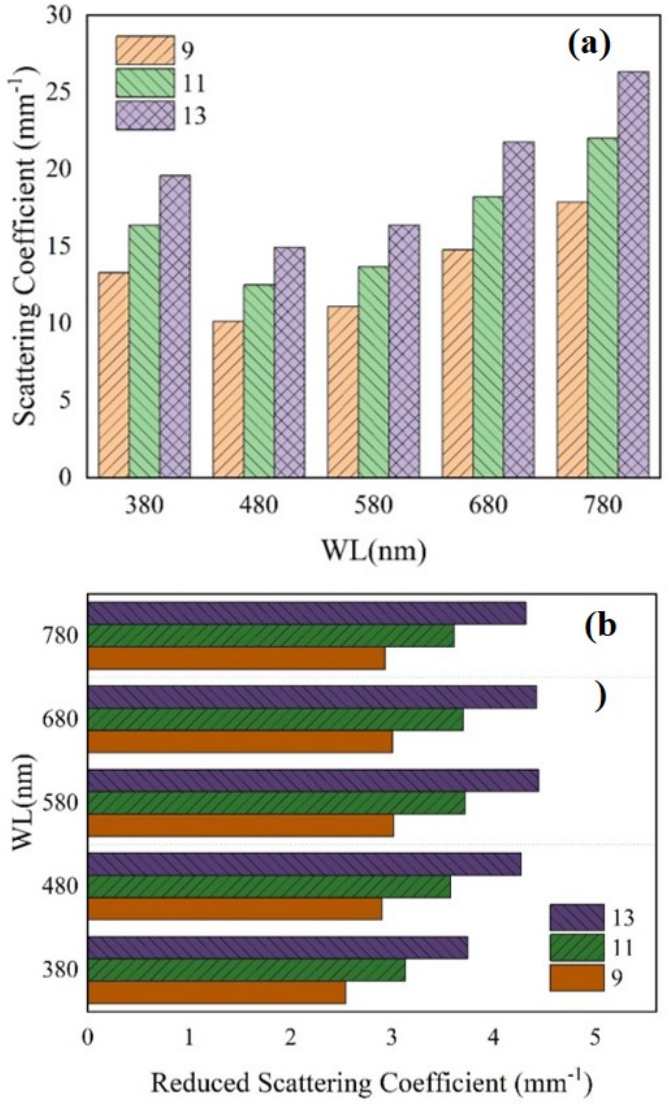

Figure 1. Scattering Coefficients with Various Wavelengths: (a) Scattering Coefficient, (b) Reduced Scattering Coefficient

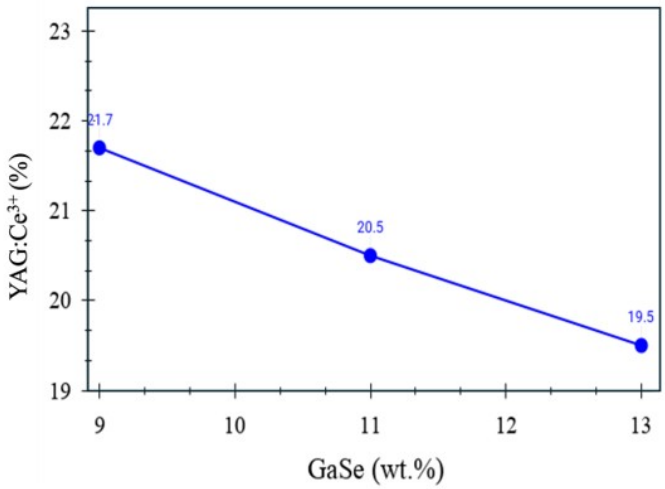

Figure 2. YGA:Ce Phosphor Proportion Values with Various GaSe Proportions

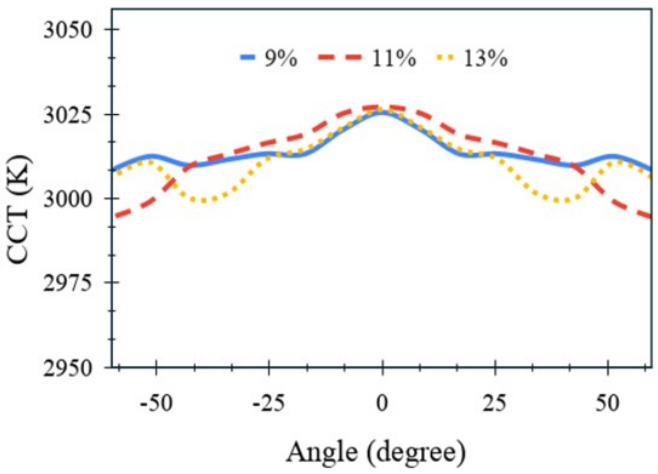

Figure 3. CCT Values with Various GaSe Proportions

The optical performance of the crystal was further validated through laser testing. Under pulsed operation, the GaSe crystal generated laser pulses with a full width at half maximum (FWHM) of approximately 20 ns and pulse energies reaching up to 1 mJ. The emitted beam was tightly concentrated utilizing a ZnSe lens, with the GaSe sample precisely positioned at the focal point to ensure optimal intensity within the nonlinear medium. The sample orientation was systematically adjusted to maximize second harmonic generation (SHG) output. The optimal incidence angle was found to be approximately 40°, corresponding to an internal propagation angle of about 14°. This value closely matches the theoretical phase-matching angle predicted for type-I SHG along the c-axis in GaSe, confirming that the fabricated crystals possess suitable orientation and homogeneity for efficient nonlinear optical conversion.

To further understand the thermal behavior influencing crystal growth, modeling of thermal transport within the growth furnace was conducted, incorporating the furnace's heating parameters and the intrinsic thermophysical properties of GaSe. The simulations indicate that purely conductive heat transfer dominates during crystal growth, which is consistent with GaSe's very low Prandtl number, signifying minimal convective influence. The calculated isothermal distributions inside the growth tube under experimental conditions reveal the evolution of the temperature field during melting and subsequent solidification. The thermal profile shows a distinct change in the temperature gradient as the material transitions from liquid to solid, requiring approximately 20 minutes for the temperature field to stabilize. The two-zone heating configuration employed in the current setup provides a stable and uniform thermal gradient, suggesting that the solid–liquid interface remains well-defined and consistent throughout the growth region. Ongoing modeling studies

are being extended to include a three-zone furnace configuration aimed at producing larger, higher-purity GaSe crystals with improved control over the solid–liquid interface and compositional uniformity.

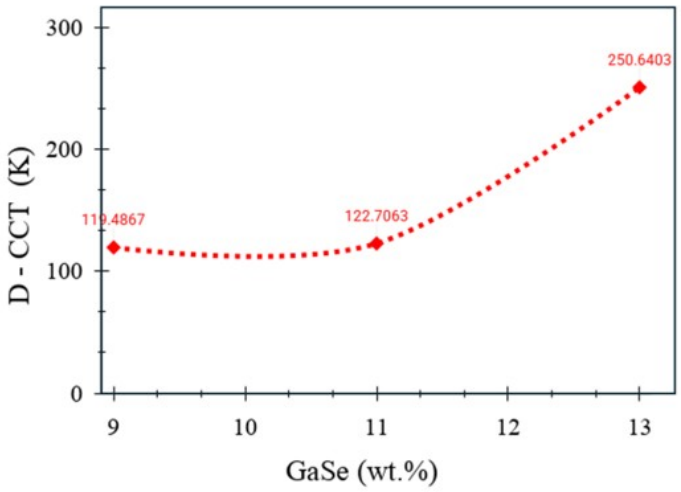

Figure 4. Color Difference Values with Various GaSe Proportions

The association among thermal simulation and nonlinear optical properties of Bridgman-grown GaSe functions via multiple intermediary mechanisms, mainly including interfacial form, thermal strain, as well as liquefy convection. Based on thermal simulations, the liquefy-crystal interfacial plane within GaSe Bridgman growth would be highly arched because of the significant thermal anisotropic factor of the sample. The interfacial divergence surges considerably alongside growth pace, whilst boosting the ampoule-wall heat gradient abates the interfacial arch. An arched interfacial plane encourages twinning as well as polytype blending. Twin as well as polytype fringes function in the form of realm barriers dispersing the pump ray as well as interrupting the phase-linking cohesion. Formational assessment via SHG angle scanning uncovers such defects and every divergence of granular sheets with greater breadth surpassing the cohesion span leads to a quantifiable alteration of SHG intenseness against angles. Simulation-oriented optimizing process for the temperature gradient for flattening the interfacial plane straightforwardly abates twinning, generating crystal granules featuring ϵ-polytype formation and subsequently greater SHG transmutation proficiency (Cong et al., 2024).

Based on simulation estimation, the local heating across the ampoule barrier may invert the flux pathway across the interfacial plane, substantially affects the allocation of dopants or impurities within the solid phase. The Prandtl number of GaSe at roughly 2.8 signifies that the liquefying flux as well as thermal transference would be highly linked and every disruption to towing or rotating pace alters the temperature allocation as well as interfacial form. Non-homogenous impurity or stoichiometric allocations generates localized variances within the

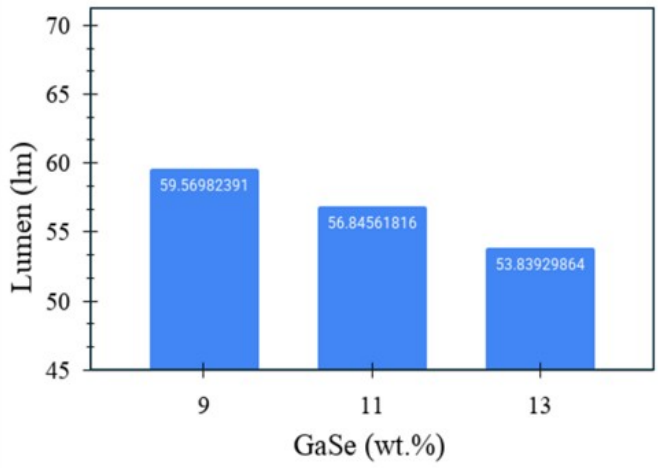

Figure 5. Luminescence Strength with Various GaSe Proportions

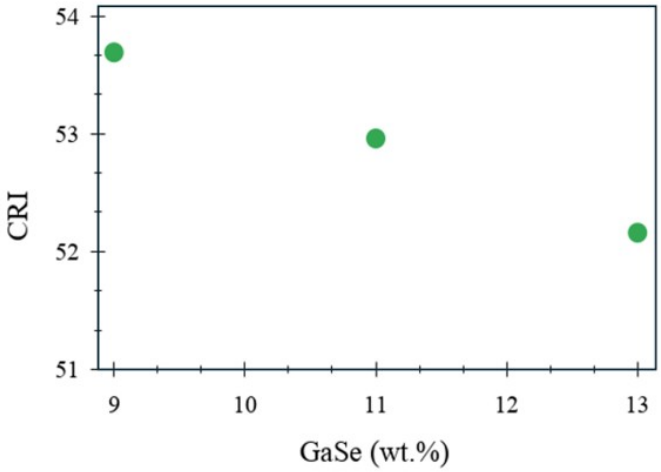

Figure 6. CRI Values with Various GaSe Proportions

refraction index as well as absorptivity coefficient. In terms of frequency transmutation, the phase-linking state necessitates refraction index homogeneity across the whole interactivity span. It was shown that the crystal granules developed within the optimal simulation furnace setting displayed a greater second harmonic transmutation coefficient that surpasses pure GaSe crystal granules developed without an optimizing process. The limited-volume simulation enables them to estimate and regulate convection profiles that may generate constitutional stripes observable in the form of absorptivity bands.

The layered formation of GaSe featuring faint van der Waals interlayer binding leads to high susceptibility towards split fracturing subject to thermal strain. Microscopic fractures as well as strain-generated delamination produce dispersion penalties which abate the interactivity span in terms of frequency transmutation. They will also yield wavefront contortion which lessens

ray performance and abate the laser- induced damage threshold, restricting the maximal utilizable pump energy. Integrated GaSe crystal granules developed using optimal simulation parameters have shown greater optical damage threshold as well as greater frequency transmutation proficiency, surpassing normally developed crystal granules.

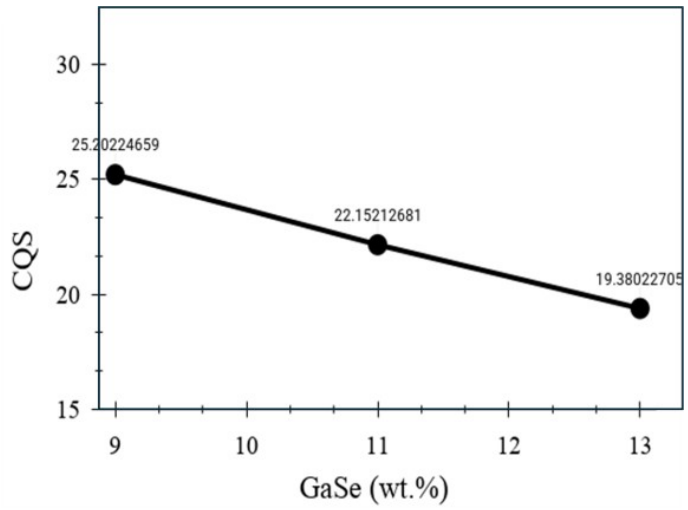

Figure 7. CQS Values with Various GaSe Proportions

While GaSe would be mainly deemed a nonlinear optical crystal, there would be notable associations among its crystal growth performance and LED optical parameters. GaSe would be a straightforward bandgap semiconductor with an opening reaching about 2.0 eV under room temperature, matching the red discharge at 620 nm, making it applicable to nonlinear frequency transmutation as well as illumination discharge settings such as LEDs, electronic ray lasers, as well as electro-optical transmuters. The identical crystalline growth parameters optimizing nonlinear optical proficiency essentially control parameters associated with LEDs. Figure 1 describes how GaSe dosage influences light dispersion, with Figures 1(a) and (b) respectively exhibiting scattering coefficient and reduced scattering coefficient, showing that GaSe enhances optical efficiency by improving wavelength converting efficiency and illumination transfer. Decreased forward spreading and reabsorption increase blue-light brightness while strengthening forward blue-light emission (My et al., 2023; Thanh Tung et al., 2023). This enhancement is achieved by decreasing the yellow-phosphor concentration and increasing the GaSe content. Likewise, the ability to adjust the correlated color temperature (CCT) remains limited, as CCT does not depend on concentration, as shown in Figures 3 and 4. As the GaSe dosage increases, the YGA:Ce yellow-phosphor content also rises, as demonstrated in Figure 2, which further shows that increasing the GaSe dosage (9–13 wt.%) decreases the YGA:Ce phosphor proportion from 21.7% to 19.5%. Figure 3 indicates that higher doping reduces CCT variance, with CCT reaching a peak of 3025 K at 11 wt.% GaSe. Figure 4 shows that the D-CCT drops to its minimum value at 9 wt.% GaSe, which is approximately 130 K lower than the peak observed at 13 wt.% GaSe (250 K).

Figure 5 indicates that GaSe does not consistently enhance the brightness of white-light emissions, with the brightest brightness occurring at 9 wt.% GaSe and the lowest at 13 wt.%. At higher GaSe concentrations, increased backscattering and reabsorption reduce blue-light emission and produce uneven hue distribution, and stronger backscattered blue light can shift the phosphor's emission from blue toward yellow or orange-red. Because the phosphor covering may solely tolerate a limited GaSe content, light interacting with surrounding objects undergoes multiple reflections, narrowing the emission spectrum (Tung et al., 2024a,b). As a result, higher phosphor loading increases the proportion of converted light reflected backward, raising the CCT whereas reducing illumination strength. Figure 5 further shows that incorporating 9 wt.% GaSe into a simulated WLED with a lumen output of nearly 60 lm enhances overall brightness and hue homogeneity.

Figures 6 and 7 additionally show that varying GaSe content influences the brightness and color rendition of white LEDs, with CRI and CQS exhibiting slight declines as the GaSe concentration rises to 13 wt.%. These reductions are likely associated with the unstable behavior of blue, green, and yellow-orange emissions, as elevated GaSe values introduce irregular illumination emission, a stronger shift toward yellow-orange hues, and raised spread. As the outcomes are evaluated, adjustments to the CRI and CQS of this phosphor will additionally consider other influencing factors such as particle size (Cong et al., 2024; Le et al., 2024).

4. CONCLUSIONS

The liquid-encapsulated Bridgman technique proved effective for producing high-quality modified GaSe crystals, yielding centimeter-scale specimens suitable for frequency-conversion uses. Preliminary measurements indicate that these altered GaSe crystals exhibit enhanced second-harmonic generation (SHG) efficiency, reflected by a higher nonlinear coefficient (d-factor) compared with unmodified GaSe, suggesting that the structural or compositional modifications introduced during growth have a positive influence on nonlinear optical performance. Building upon these encouraging results, initial computational modeling is now being used to inform the development of an improved thermal system designed to maintain a fully isothermal solid–liquid interface throughout the growth zone. Achieving such thermal uniformity is expected to further minimize defect formation, promote compositional homogeneity, and ultimately support the fabrication of even higher-quality GaSe crystals optimized for advanced nonlinear optical technologies.

5. ACKNOWLEDGEMENT

The authors wishes to express their gratitude to the Posts and Telecommunications Institute of Technology, Vietnam, for financial support for this research.

REFERENCES

Anh, N. D. Q., S. D. Ho, P. T. M. Man, T. K. Duy, and N. T. P. Loan (2025a). Obtaining Higher LED's Lighting Chromaticity and Luminosity with SiO_2 Particles at Different Diameters. *Journal of Advanced Engineering and Computation*, **9**(1); 21–28

Anh, N. D. Q., N. T. P. Loan, P. Van De, and H. Lee (2025b). Potassium Bromide Scattering Simulation for Improving Phosphor-Converting White LED Performance. *Optoelectronics and Advanced Materials: Rapid Communications*, **19**(7–8); 378–383

Chen, M.-J., N. T. P. Loan, L. Van Tho, T. M. Bui, P. X. Le, N. D. Q. Anh, H.-Y. Liao, J.-C. Chang, and H.-Y. Lee (2020). The Impacts of $Ba_2Li_2Si_2O_7$:Sn^{2+},Mn^{2+} and $CaMgSi_2O_6$:Eu^{2+},Mn^{2+} Particles on the Optical Properties of Remote Phosphor LED. *Materials Science-Poland*, **38**(1); 197–205

Cong, P. H., L. X. Thuy, N. T. P. Loan, H. Y. Lee, and N. D. Q. Anh (2024). ZnO-Doped Yellow Phosphor Compound for Enhancing Phosphor-Conversion Layer's Performance in White LEDs. *Optoelectronics and Advanced Materials - Rapid Communications*, **18**; 389–395

Dang, H., N. Loan, N. Thi Kim Chung, and N. D. Quoc Anh (2021a). The Study of Convex-Dual-Layer Remote Phosphor Geometry in Upgrading WLEDs Color Rendering Index. *International Journal of Electrical and Computer Engineering*, **11**; 3890–3896

Dang, N., D. Nguyen, T. Nguyen, D. Nguyen, and H.-Y. Lee (2021b). Enhance WLEDs Performance with Additional Phosphor Materials in Multi-Layer Remote Structure. *Journal of Advanced Engineering and Computation*, **5**; 167

Hanh, N., N. Loan, and N. D. Quoc Anh (2020). The Application of Green YPO_4:Ce^{3+},Tb^{3+} and Red $LiLaO_2$:Eu^{3+} Layers to Remote Phosphor LED. *TELKOMNIKA (Telecommunication Computing Electronics and Control)*, **18**; 3216

Hanh, N., P. That, and N. D. Quoc Anh (2021a). Eu^{2+}-Activated Strontium-Barium Silicate: A Positive Solution for Improving Luminous Efficacy and Color Uniformity of White Light-Emitting Diodes. *Materials Science-Poland*, **38**(4); 594–600

Hanh, N., P. That, N. D. Quoc Anh, and T. Trang (2021b). Triple-Layer Remote Phosphor Structure: A Novel Option for the Enhancement of WLEDs' Color Quality and Luminous Flux. *Materials Science-Poland*, **38**; 654–660

Le, P., S. Ho, N. D. Quoc Anh, and H.-Y. Lee (2022). Triple-Layer Remote Phosphor Structure: A Potential Packaging Configuration to Enhance Both Color Quality and Lumen Efficiency of 6,000–8,500 K WLEDs. *Materials Science-Poland*, **39**; 458–466

Le, P. X., N. D. Q. Anh, and H. Y. Lee (2024). Regulating the White LED Properties with Different SiO_2 Particle Sizes. *Optoelectronics and Advanced Materials - Rapid Communications*, **18**; 485–489

Le, P. X., N. T. P. Loan, and N. D. Q. Anh (2026). Optical Assessment of Titanium Oxide Employed in Phosphor-Transmuted WLED Devices. *Science and Technology Indonesia*, **11**(1); 345–355

Le, P. X., N. T. P. Loan, N. D. Q. Anh, and H.-Y. Lee (2025). Thermally Stable Sol-Gel Yttrium Aluminum Garnet Cerium Phosphors for White Light-Emitting Diodes. *International Journal of Advances in Applied Sciences*, **14**(4); 1367

Loan, N., N. D. Quoc Anh, N. Trang, and H.-Y. Lee (2022). Better Color Distribution Uniformity and Higher Luminous Intensity for LED by Using a Three-Layered Remote Phosphor Structure. *Materials Science-Poland*, **40**; 60–67

Loan, N. T. P. and N. D. Q. Anh (2020a). $LaSiO_3Cl$:Ce^{3+},Tb^{3+} and Mg_2TiO_4:Mn^{4+}: Quantum Dot Phosphors for Improving the Optical Properties of WLEDs. *International Journal of Electrical and Computer Engineering*, **10**(5); 5191–5197

Loan, N. T. P. and N. D. Q. Anh (2020b). $Na_3Ce(PO_4)_2$:Tb^{3+} and $Na(Mg_2\text{-}xMnx)LiSi_4O_{10}F_2$:Mn Phosphors: A Suitable Selection for Enhancing Color Quality and Luminous Flux of Remote White Light-Emitting Diodes. *TELKOMNIKA (Telecommunication Computing Electronics and Control)*, **18**(4); 2095

Loan, N. T. P. and N. D. Q. Anh (2020c). The Effects of ZnO Particles on the Color Homogeneity of Phosphor-Converted High-Power White LED Light Sources. *International Journal of Electrical and Computer Engineering (IJECE)*, **10**(5); 5155–5161

Loan, N. T. P., N. D. Q. Anh, P. T. M. Man, and H.-Y. Lee (2025). Assessing Thermic Degradation for Yttrium–Aluminum Precursive Agents Applied to YAG Phosphor Samples. *Science and Technology Indonesia*, **10**(4); 1209–1214

Luo, G.-F., N. Loan, L. Tho, N. D. Quoc Anh, and H.-Y. Lee (2020). Enhancement of Color Quality and Luminous Flux for Remote-Phosphor LEDs with Red-Emitting $CaMgSi_2O_6$:Eu^{2+},Mn^{2+}. *Materials Science-Poland*, **38**(3); 409–415

My, L., N. Thai, T. M. Bui, H.-Y. Lee, and N. D. Quoc Anh (2023). Phosphor Conversion for WLEDs: YBO_3:Ce^{3+},Tb^{3+} and Its Effects on the Luminous Intensity and Chromatic Properties of Dual-Layer WLED Model. *Materials Science-Poland*, **40**; 105–113

Nguyen, V. D. and D. Q. A. Nguyen (2025). $Ba_3GdNa(PO_4)_3F$:Eu^{2+} Phosphor with Blue-Red Emission Colors on White-LED Properties. *Indonesian Journal of Electrical Engineering and Computer Science*, **38**(3); 1564–1571

Pham, T., N. Phan, G.-F. Luo, H.-Y. Lee, and D. Nguyen (2021). The Application of Calcium Carbonate $CaCO_3$ and Titania TiO_2 for Color Homogeneity and Luminous Flux Enhancement in PC-LEDs. *Journal of Advanced Engineering and Computation*, **5**; 75

Thanh Trang, T. (2022). Comparison Between SEPs of $CaCO_3$ and TiO_2 in Phosphor Layer for Better Color Uniformity and Stable Luminous Flux of WLEDs with 7,000 K. *Materials Science-Poland*, **40**; 1–8

Thanh Tung, H., D. Thi, and N. Anh (2023). The Effects of $Ca_{14}Mg_2(SiO_4)_8$:Eu^{2+} Phosphor on White Light Emission Quality of LED-Phosphor Packages. *Bulletin of Electrical Engineering and Informatics*, **12**; 3388–3394

That, P., N. Loan, L. Tho, N. D. Quoc Anh, H.-Y. Liao, G.-F. Luo, and H.-Y. Lee (2021). Enhancing Color Quality of WLEDs with Dual-Layer Remote Phosphor Geometry. *Materials Science-Poland*, **38**; 667–674

That, P. T., T. M. Bui, N. T. P. Loan, P. X. Le, N. D. Q. Anh, and

L. V. Tho (2020). Dual-Layer Remote Phosphor Structure: A Novel Technique to Enhance the Color Quality Scale and Luminous Flux of WLEDs. *International Journal of Electrical and Computer Engineering*, **10**(4); 4015–4022

Thi, M. H. N., T. M. Bui, and N. D. Q. Anh (2021). Aiming to the Superior of Phosphor Pattern: Influence of SiO_2 Nanoparticles on Photoluminescence Intensification of YAG:Ce. *International Journal of Electrical and Computer Engineering*, **11**(6); 4833–4839

Tran, A.-M., N. D. Quoc Anh, and N. Loan (2020a). The Influences of Calcium Fluoride and Silica Particles on Improving Color Homogeneity of WLEDs. *TELKOMNIKA (Telecommunication Computing Electronics and Control)*, **18**; 2696

Tran, A.-M. D., N. D. Q. Anh, and N. Thi Phuong Loan (2020b). Enhancing Light Sources Color Homogeneity in High-Power Phosphor-Based White LED Using ZnO Particles. *TELKOMNIKA (Telecommunication Computing Electronics and Control)*, **18**(5); 2628

Tran, T., N. D. Quoc Anh, and N. Loan (2020c). Comparison of Calcium Carbonate and Titania Particles on Improving Color Homogeneity and Luminous Flux of WLEDs. *TELKOMNIKA (Telecommunication Computing Electronics and Control)*, **18**; 2690

Trang, L. T. and N. D. Q. Anh (2025). Influences from SiO_2 Particles on Optical Properties of White Diodes Verified Through Computer Simulation. *Indonesian Journal of Electrical Engineering and Computer Science*, **38**(3); 1572–1579

Tung, H., N. Anh, H. Lee, et al. (2024a). Impact of Phosphor Granule Magnitudes as Well as Mass Proportions on the Luminous Hue Efficiency of a Coated White Light-Emitting Diode and One Green Phosphor Film. *Optoelectronics and Advanced Materials-Rapid Communications*, **18**(January-February 2024); 58–65

Tung, H. T., B. T. Minh, N. L. Thai, H. Y. Lee, and N. D. Q. Anh (2024b). ZnO Particles as Scattering Centers to Optimize Color Production and Lumen Efficiencies of Warm White LEDs. *Optoelectronics and Advanced Materials - Rapid Communications*, **18**; 283–288

